

XMM-Newton and *Swift* observations prove GRB 090709A to be a distant, standard, long GRB

A. De Luca,^{1,2*} P. Esposito,^{2,3} G. L. Israel,⁴ D. Götz,⁵ G. Novara,² A. Tiengo² and S. Mereghetti²

¹IUSS - Istituto Universitario di Studi Superiori, viale Lungo Ticino Sforza 56, 27100 Pavia, Italy

²INAF/Istituto di Astrofisica Spaziale e Fisica Cosmica - Milano, via E. Bassini 15, 20133 Milano, Italy

³Istituto Nazionale di Fisica Nucleare, sezione di Pavia, via A. Bassi 6, 27100 Pavia, Italy

⁴INAF/Osservatorio Astronomico di Roma, via Frascati 33, 00040 Monteporzio Catone, Italy

⁵CEA Saclay, DSM/Irfu/Service d'Astrophysique, Orme des Merisiers, Bât. 709, 91191 Gif-sur-Yvette, France

Accepted 2009 November 09. Received 2009 November 03; in original form 2009 October 15

ABSTRACT

GRB 090709A is a long gamma-ray burst (GRB) discovered by *Swift*, featuring a bright X-ray afterglow as well as a faint infrared transient with very red and peculiar colors. The burst attracted a large interest because of a possible quasi-periodicity at $P = 8.1$ s in the prompt emission, suggesting that it could have a different origin with respect to standard, long GRBs. In order to understand the nature of this burst, we obtained a target of opportunity observation with *XMM-Newton*. X-ray spectroscopy, based on *XMM-Newton* and *Swift* data, allowed us to model the significant excess in photoelectric absorption with respect to the Galactic value as due to a large column density ($\sim 6.5 \times 10^{22} \text{ cm}^{-2}$) in the GRB host, located at $z \sim 4.2$. Such a picture is also consistent with the infrared transient's properties. Re-analysis of the prompt emission, based on *INTEGRAL* and on *Swift* data, excludes any significant modulation at $P = 8.1$ s. Thus, we conclude that GRB 090709A is a distant, standard, long GRB.

Key words: gamma-rays: bursts – X-rays: bursts – X-rays: individual: GRB 090709A.

1 INTRODUCTION

The bright, long GRB 090709A was discovered by the Burst Alert Telescope (BAT) onboard *Swift* on 2009 July 9 at $T_0 = 07:38:34.59$ UT (Morris et al. 2009). The prompt emission had a complex structure (see Fig. 1), with a multi-peaked light curve lasting $t_{90} \sim 89$ s. The peak flux was $7.8 \pm 0.3 \text{ ph cm}^{-2} \text{ s}^{-1}$ at $T_0 + 21$ s and the fluence was $(2.57 \pm 0.03) \times 10^{-5} \text{ erg cm}^{-2}$ in the 15–350 keV energy range (Sakamoto et al. 2009). A bright X-ray afterglow was observed by the X-ray Telescope (XRT) onboard *Swift* starting as soon as 77 s after the trigger (Morris et al. 2009). Analysis of XRT data up to $T_0 + 0.3$ days yielded evidence for a break in the decay at $T_0 + 0.1$ days. The XRT spectrum was described by a power law with an absorbing column exceeding by a factor ~ 3 the Galactic value in the direction of GRB 090709A (Rowlinson & Morris 2009).

On the optical/infrared side, several follow-up observations of the field of GRB 090709A were performed. A possible, faint transient with very red colors was detected in early observations in the near infrared, performed within a few minutes from T_0 by automated instruments such as the PAIRITEL Telescope (Morgan, Bloom & Klein 2009), the Palomar Observatory's 60-inch telescope (Cenko et al. 2009) as well as the Faulkes North

Telescope (Guidorzi et al. 2009). The peculiar colors of such a transient prompted to suggest a very high redshift ($z \sim 10$) for such GRB. The same infrared source was possibly detected in a Subaru image collected ~ 2 hours after the trigger (Aoki et al. 2009). A very deep observation performed with the 10.4 m Gran Telescopio CANARIAS telescope ~ 41 hours after the GRB detected no source at the same position, down to a 3σ upper limit $I > 25.5$ (Castro-Tirado et al. 2009).

GRB 090709A attracted much interest because of a very peculiar timing phenomenology. Markwardt et al. (2009) reported evidence for quasi-periodical pulsations at ~ 8 s in the prompt emission, based on analysis of *Swift*/BAT data in the 15–350 keV energy range. Such a quasi-periodicity was then confirmed by the analysis of Konus-Wind and Konus-RF data (Golenetskii et al. 2009), as well as by analysis of *INTEGRAL*/ACS data (Götz et al. 2009). Taken at face value, such a result is tantalizing. This would be the first detection of periodic activity in the prompt gamma-ray emission of a GRB, which could yield rare information on the behavior of the central engine.

Indeed, the peculiar quasi-periodicity immediately prompted several authors (e.g. Markwardt et al. 2009 and Guidorzi et al. 2009) to suggest that GRB 090709A could be different in origin with respect to standard long GRBs, and possibly related to activity of a magnetar, either within the Galaxy, or extragalactic. However, a search for pulsations in early afterglow data collected by

* E-mail: deluca@iasf-milano.inaf.it

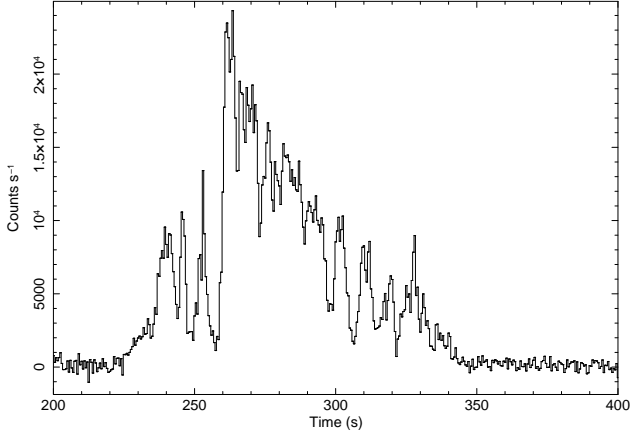


Figure 1. Light curve of GRB 090709A obtained with the *Swift*/BAT in the 15–350 keV. The time binning is 0.5 s.

Swift/XRT yielded null results (Mirabal & Gotthelf 2009).

To shed light on the nature of the peculiar GRB 090709A we asked for an *XMM-Newton* Target of Opportunity (ToO) observation, aimed at characterizing the afterglow emission at a later stage (about 2 days after the event), when the target is too faint to be studied with *Swift*/XRT. Here we report on the outcome of the *XMM-Newton* ToO, which, coupled to a re-analysis of *Swift* and *INTEGRAL* data, allowed us to obtain a comprehensive description of the high-energy phenomenology of GRB 090709A.

2 IS THE X-RAY AFTERGLOW “PECULIAR”?

2.1 The *XMM-Newton* view of GRB 090709A

The ToO observation started on 2009 July 11 at 07:56:50 UTC (48.3 hr after the burst) and lasted 24.5 ks. All the EPIC cameras were operated in Full Frame mode (imaging across the whole field of view, with a time resolution of 73 ms and 2.6 s in the pn and in the two MOS cameras, respectively), using the thin optical filter. We processed Observation Data Files using the most recent release of the *XMM-Newton* Science Analysis Software (SASv9.0).

No significant particle background episodes affected the observation. The afterglow is clearly detected in all of the EPIC cameras. The position, RA = 19^h19^m42^s.6, Dec. = +60°43′35″.0 (J2000), with a 1σ error of 1″.5, is consistent with the XRT position (Osborne et al. 2009).

Source photons were selected from a circular region (30 arcsec radius) centered on the target. Background events were extracted from a source-free region in the same chip as the target. The source average background-subtracted count rate in the 0.3–8 keV energy range is 0.155 ± 0.003 counts s⁻¹, 0.051 ± 0.002 counts s⁻¹ and 0.048 ± 0.002 counts s⁻¹ in the pn, MOS1 and MOS2 cameras, respectively. Background contributes ~5% more counts in the extraction region.

2.1.1 Search for pulsations

As a first step, after correcting photon arrival times to the solar system’s barycenter using the task BARYCEN, we searched for pulsations in the GRB afterglow using two methods. First, we used the Z_n^2 test (Buccheri et al. 1983), with the number of harmonics n being varied from 1 to 2. Second, a Fourier analysis of the light-curves was performed using the method described in Israel & Stella

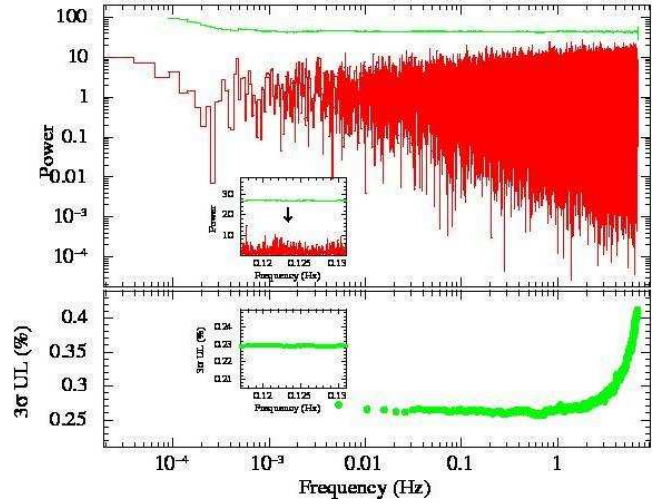


Figure 2. Results of the timing analysis on EPIC/pn data (0.5–10 keV), collected ~48 hours after the trigger. Upper panel: the power spectrum is shown together with the threshold for the detection of sinusoidal signals at the 3σ confidence level. Lower panel: upper limits on the pulsed fraction. See text for details.

(1996). The analysed period range spans from 150 ms up to 10^4 s (~262 000 total period trials). No significant (periodic or quasi-periodic) signal was found with either method, searching the whole period range or restricting the search around the 8 s hypothetical period. The upper limits on the pulsed fraction, computed according to Vaughan et al. (1994), are shown in Figure 1 as a function of the frequency (the curves refer to the 3σ upper limits on the sinusoid semi-amplitude pulsed fraction in the 0.5–10 keV energy range). Upper limits at the 8 s hypothetical period range between 26% when considering all the Fourier frequencies in the whole spectrum and 23% for the narrower search (see insets in Figure 2, lower panel).

2.1.2 Spectral analysis

Source spectra were rebinned in order to oversample the instrumental energetic resolution by a maximum factor 3, or to have at least 25 counts per bin. Ad-hoc response matrices and effective area files were generated using the SAS tasks RMFGEN and ARFGEN, respectively.

Spectral analysis was performed using the XSPEC software (v12.4.0). Errors on spectral parameters are given at the 90% confidence level for a single parameter of interest. Simultaneous modelling of pn, MOS1 and MOS2 spectra with an absorbed power law model results in a rather poor fit ($\chi^2_\nu = 1.52$, 152 d.o.f.). The best fit photon index is $\Gamma = 2.15 \pm 0.05$, while the absorbing column ($N_H = (2.5 \pm 0.2) \times 10^{21}$ cm⁻²) is significantly larger than the Galactic value in the direction of GRB 090709A ($\sim 6.7 \times 10^{20}$ cm⁻², according to Dickey & Lockman 1990). Such result are in broad agreement with the XRT ones reported by Rowlinson & Morris (2009).

We then added to the Galactic absorption component (with N_H fixed to 6.7×10^{20} cm⁻²) a redshifted absorption component $N_{H,z}$ (abundances were set to Solar values). This model yields a much better description of the data ($\chi^2_\nu = 1.11$, 151 d.o.f.). The resulting photon index is $\Gamma = 2.00 \pm 0.05$. The fit gives a very large intrinsic column density $N_{H,z} = (9.7 \pm 2.0) \times 10^{22}$ cm⁻², while the redshift is constrained to 5.1 ± 0.4 . The time-averaged,

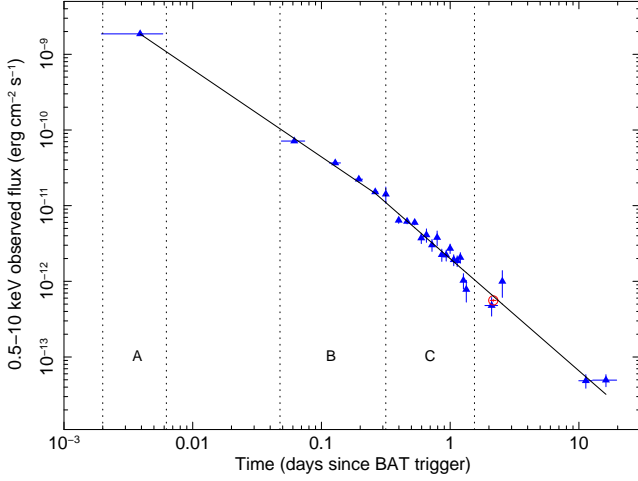


Figure 3. Soft X-ray light-curve of GRB 090709A spanning the time range from $T_0 + 77$ s to $T_0 + 20$ days. Blue triangles: *Swift*/XRT data; Red circle: *XMM-Newton* data. The broken power law best describing the flux decay is superimposed. Time intervals for XRT time-resolved spectroscopy are marked as A, B, and C.

observed flux is 5.6×10^{-13} erg cm $^{-2}$ s $^{-1}$ in the 0.5–10 keV energy range.

2.2 Swift/XRT data

In order to put the *XMM-Newton* observation in context, we retrieved and analysed the XRT observations of the afterglow. The XRT CCD detector (0.2–10 keV) started observing the field of GRB 090709A only 77 s after the BAT trigger. Table 1 reports the log of this and the subsequent XRT follow-up observations, performed in both photon counting (pc) and windowed timing (wt) modes,¹ that were used for this work (some wt observations last only a few seconds and we did not include them in our analysis).

The data were processed with standard procedures (XRTPIPELINE version 0.12.3), filtering, and screening criteria by using FTOOLS in the HEASOFT package (ver. 6.6). For the timing and spectral analyses, we extracted the pc source events from a circle with a radius of 20 pixels (one pixel corresponds to about $2''.36$) and the wt data from a 40×40 pixels box along the image strip. To estimate the background, we extracted pc and wt events from source-free regions far from the position of GRB 090709A.

The overall light curve of the afterglow of GRB 090709A is shown in Fig. 3. Count rates (for both *Swift*/XRT and *XMM-Newton*/EPIC) have been converted into fluxes using the best-fitting spectral models described below and in the previous section. The flux decays as a broken power law. The break occurs at 0.26 ± 0.05 days after the GRB, when the index of the decay changes from -1.15 ± 0.01 to -1.48 ± 0.05 .

¹ In pc mode the entire CCD is read every 2.507 s, while in wt mode only the central 200 columns are read and only one-dimensional imaging is preserved, achieving a time resolution of 1.766 ms (see Hill et al. 2004 for more details).

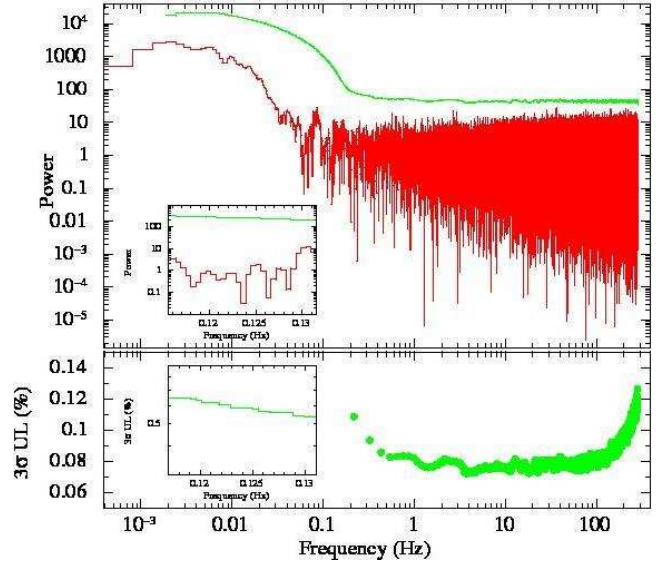


Figure 4. Same as Fig. 2, using the data collected with *Swift*/XRT (0.5–10 keV) in WT mode in the early afterglow phase (from $T_0 + 77$ s to $T_0 + 539$ s).

2.2.1 Search for pulsations

We calculated the power spectrum for the first *Swift* dataset during which the time resolution was higher (WT mode) and with large enough statistics. The analysed period range spans from 4 ms up to 10^3 s ($\sim 262\,000$ total period trial) approximatively. Also in this case no significant signal was found searching the whole period range or restricting the search around the 8 s signal. Due to the presence of low-frequency noise (introduced by the source rapid decay during the *Swift* observation), meaningful upper limits in the range 60%–50% have been inferred only for the narrow search. The subtraction of high-order de-trending polynomials (taking account for the source rapid decay) does not change significantly the above results. We note the presence of a low-significance ($\sim 2\sigma$) QPO-like feature in the power spectrum around 11 s.

2.2.2 Spectral analysis

We extracted time-resolved spectra of the afterglow. In order to have a good photon statistics, we combined data collected within the three time intervals marked as A, B, and C in Fig. 3.

A simple, absorbed power-law model does not reproduce well the spectra and results in a N_H column significantly larger than the Galactic value. As in the *XMM-Newton* case, we added a redshifted absorption component, which yielded a much better fit to the data. Results are reported in Table 2.

In order to assess the possible spectral evolution as a function of time, we generated confidence ellipses for z vs. $N_{H,z}$ and for Γ vs. $N_{H,z}$ for the three datasets having the largest photon statistics (XRT A, XRT B and EPIC). As shown in Fig. 5, the strong correlation between the $N_{H,z}$ and z parameters prevents from concluding that we are observing different values in different epochs. Conversely, a significant softening of the power law component is apparent. The photon index varies from ~ 1.7 in the early afterglow phase to ~ 2 at the time of the *XMM-Newton* observation.

Indeed, fitting the above model simultaneously to all XRT and EPIC spectra, leaving the power law as the only spectral component free to vary as a function of the epoch, yields a very good result

Table 1. Journal of the *Swift*/XRT observations. The *Swift*/BAT trigger time is 2009-07-09 07:38:35 UT.

Sequence/Mode	Start/End time (UT) yyyy-mm-dd hh:mm:ss		Exposure ^a (ks)	Net average count rate ^b (counts s ⁻¹)
00356890000/wt	2009-07-09 07:39:52	2009-07-09 07:47:33	0.4	35.4 ± 0.3
00356890000/pc	2009-07-09 08:47:09	2009-07-09 15:14:03	8.9	0.744 ± 0.009
00356890001/pc	2009-07-09 16:56:40	2009-07-09 02:29:10	7.9	0.103 ± 0.004
00356890002/pc	2009-07-10 02:34:55	2009-07-10 20:40:56	10.2	0.036 ± 0.002
00356890259/wt	2009-07-11 04:14:24	2009-07-11 15:39:27	12.0	0.008 ± 0.003
00356890003-4-5/pc	2009-07-19 06:56:06	2009-07-21 23:38:57	30.4	0.0011 ± 0.0002
00356890006-7-9-10-11/pc	2009-07-22 02:39:01	2009-07-28 22:45:58	53.4	0.0012 ± 0.0002

^a The exposure time is usually spread over several snapshots (single continuous pointings at the target) during each observation.

^b In the 0.5–10 keV energy band.

Table 2. Results of time-resolved spectroscopy with *Swift*/XRT and XMM-Newton/EPIC.

	<i>Swift</i> /XRT A	<i>Swift</i> /XRT B	<i>Swift</i> /XRT C	XMM-Newton/EPIC
Exp.Time (ks)	0.4	8.9	17.9	18.5 ^a /22.6 ^b
Mean epoch (MJD)	55021.322	55021.500	55022.248	55023.480
N_{H} (cm ⁻² , fixed)	6.7×10^{20}	6.7×10^{20}	6.7×10^{20}	6.7×10^{20}
$N_{\text{H},z}$ (cm ⁻²)	$(6.2 \pm 1.1) \times 10^{22}$	$(8.7 \pm 1.7) \times 10^{22}$	$(7.1^{+6.8}_{-3.5}) \times 10^{22}$	$(9.7 \pm 2.2) \times 10^{22}$
z	4.1 ± 0.3	4.3 ± 0.3	3.9 ± 1.0	5.1 ± 0.5
Γ	1.69 ± 0.03	1.84 ± 0.05	2.05 ± 0.14	2.00 ± 0.06
χ^2_{ν}	1.13	0.98	1.12	1.12
d.o.f.	291	172	39	151
F ^c (erg cm ⁻² s ⁻¹)	1.6×10^{-9}	3.7×10^{-11}	1.6×10^{-12}	5.6×10^{-13}

^{a/b} pn/MOS.

^c Observed flux in the 0.5–10 keV energy band.

($\chi^2_{\nu} = 1.08$, 671 d.o.f.). Such an exercise yields a best fit redshift $z = 4.2 \pm 0.2$ and intrinsic absorption $N_{\text{H},z} = (6.5 \pm 1.5) \times 10^{22}$ cm⁻², while the epoch-dependent values of Γ and of the power-law normalization are very similar to the ones reported in Table 2. Taking into account the correlation between z and $N_{\text{H},z}$, as well as the dependence of such parameters on the value of the Milky Way column density², the 90% confidence level interval turn out to be $3.7 < z < 4.5$ and 4.8×10^{22} cm⁻² $< N_{\text{H},z} < 7.7 \times 10^{22}$ cm⁻². We also note that such results are computed assuming Solar abundances in the redshifted absorber model.

3 ANY PERIODICITY IN THE PROMPT EMISSION?

Facing with a rather standard X-ray afterglow, we have studied the prompt emission in order to assess the significance of the claimed quasi-periodical variations.

3.1 *Swift*/BAT data

The coded-mask Burst Alert Telescope (BAT) onboard *Swift* collected event data (15–350 keV, with 0.1 ms time resolution) from GRB 090709A in the time range from $T_0 - 170$ s to $T_0 + 612$ s. We retrieved the event list from the *Swift* archive. After correcting

photons' time of arrival to the solar system barycenter, we generated a background-subtracted light curve in the 15–150 keV energy range using the mask-weighting technique (Senziani et al. 2007). Then, we used a procedure similar to that already discussed for XMM-Newton and *Swift*/XRT data. We searched for possible signals in the power spectrum. In this case we considered the whole set of Fourier frequencies. We searched for significant signals in the range from 20 ms to 50 s, approximately. We also included high-order de-trending polynomials to “rectify” (trend subtraction mode was selected) the light curve and minimize the low-frequency noise. Fig. 6 shows our best-case power spectrum, obtained after de-trending the light curve by using a third order polynomial. No significant signal was found, while a 3σ upper limits in the 15%–25% range was obtained in the period interval between 5 s and 15 s. We note that a peak at about 0.125 Hz, consistent to the reported period of 8 s, is present in the spectrum. The corresponding power estimate is very close to the 3σ detection threshold.

We also studied the time-averaged spectrum of the prompt emission, generating a background-subtracted spectrum with the mask-weighting technique (Senziani et al. 2007), considering the time interval from T_0 to $T_0 + 150$ s. The best fit model is a power law with photon index $\Gamma = 1.28 \pm 0.02$. The fluence in the 15–150 keV energy range is 2.38×10^{-5} erg cm⁻². Our results are fully consistent to the ones by Sakamoto et al. (2009).

3.2 INTEGRAL SPI/ACS data

The Anti-Coincidence Shield (ACS) of the Spectrometer on INTEGRAL (SPI) is routinely used as a nearly omni-directional detector

² Stratta et al. (2004) showed that a reasonable guess of the uncertainty affecting Galactic column density estimates is $\sim 30\%$ at $\sim 90\%$ confidence level.

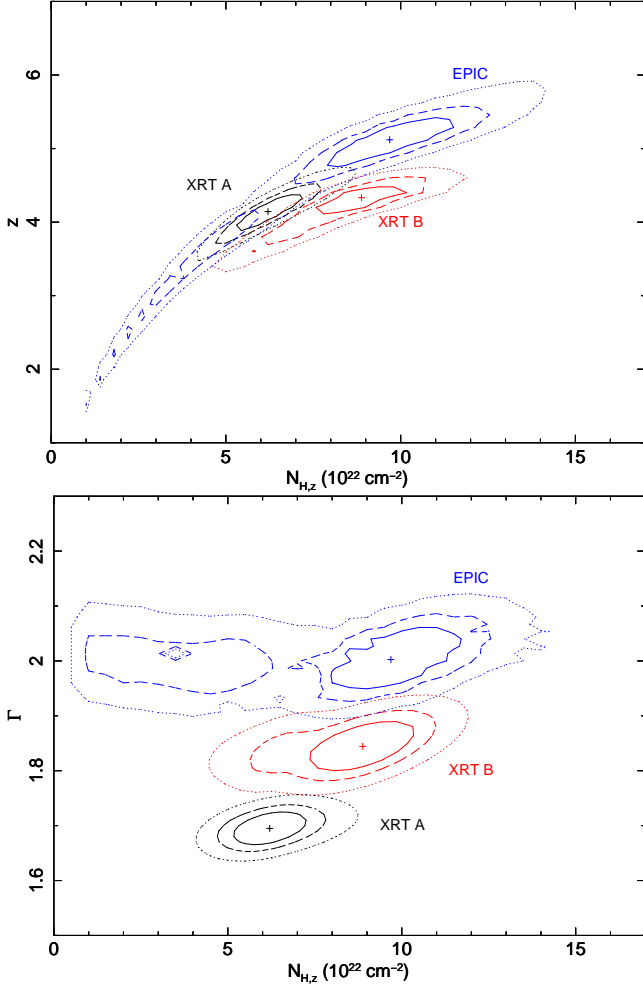


Figure 5. Upper panel: confidence contours (solid: 68%, dashed: 90%, dotted: 99%) for the redshift z vs. the intrinsic column density $N_{H,z}$. Lower panel: confidence contours (solid: 68%, dashed: 90%, dotted: 99%) for the photon index Γ vs. the intrinsic column density $N_{H,z}$.

for gamma-ray bursts (von Kienlin et al. 2003), besides serving its main function as a veto for the SPI spectrometer. The ACS provides light curves binned at 50 ms, but without energy and directional information. The low energy threshold is about 80 keV.

GRB 090709A was located at an angle $\theta = 70^\circ$ from the SPI pointing direction, resulting in an optimal response for the ACS, which is most sensitive for directions orthogonal to the satellite pointing axis.

In order to look for a possible periodic signal in the ACS data we performed the same analysis as in the *Swift*/BAT case (see above). The results are shown in Fig. 7: also in this case the search was negative. The 3σ upper limits to any pulsed signal around 0.125 Hz is 20%, and 6% and 8% for the blind search and the narrow search in the 5–15 s period interval, respectively.

4 DISCUSSION AND CONCLUSIONS

4.1 The afterglow of a distant, standard, long GRB

Prompted by early reports of the detection of a strong quasi-periodical signal in the prompt emission of GRB 090709A, we have performed a ToO observation with *XMM-Newton*.

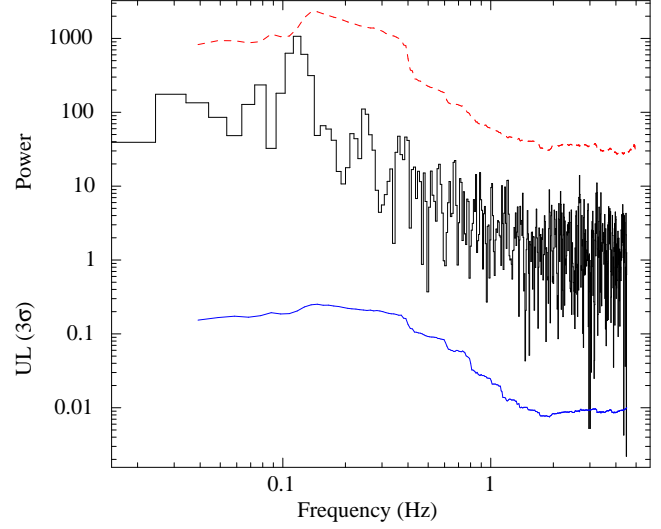


Figure 6. Similar to Fig. 2 for the prompt emission, using *Swift*/BAT data (15–150 keV) in the time range from T_0 s to $T_0 + 100$ s. The uppermost line (stepped) marks the threshold for the detection of sinusoidal signals at the 3σ c.l., while the lower one shows the corresponding upper limits on the pulsation amplitude.

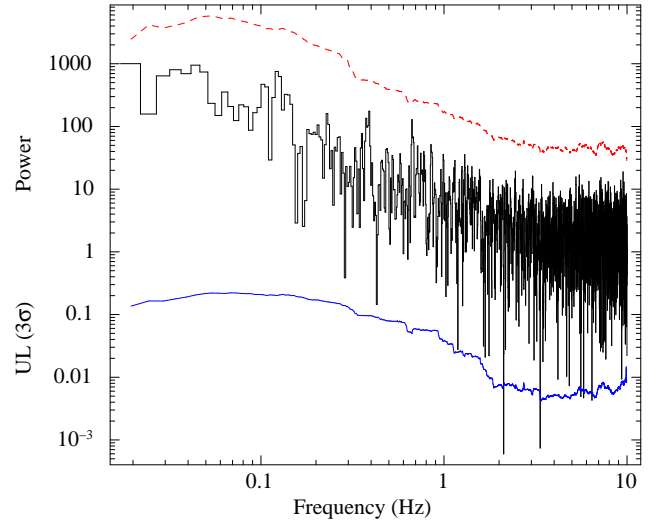


Figure 7. Similar to Fig. 6 but for the prompt emission as seen by *INTEGRAL*/SPI-ACS. The uppermost line (stepped) marks the threshold for the detection of sinusoidal signals at the 3σ c.l., while the lower one shows the corresponding upper limits on the pulsation amplitude.

The afterglow of GRB 090709A as seen in soft X-rays with the EPIC instrument, is fully similar to other cases of typical, well-behaving, long GRBs. No pulsations are seen in the X-ray emission ~ 48 hr after the trigger, with a 3σ upper limit of 15–25% on the pulsed fraction, assuming a sinusoidal pulse shape. The energy spectrum has a typical power-law shape, with a remarkable excess in photoelectric absorption (by a factor ~ 4) with respect to the Galactic N_H in the direction of GRB 090709A.

Such a picture of a “standard” X-ray afterglow is completed by *Swift*/XRT observations, which started as soon as 77 s after the burst, and extended up to 20 days after the trigger. GRB 090709A turns out to have a rich phenomenology, featuring - in addition to the intrinsic photoelectric absorption - a clear spectral evolution (the photon index Γ steepens from 1.7 to 2.0 in ~ 2 days), as well as a

break in the flux decay, with a ~ 0.3 variation in the power law decay index occurring ~ 0.26 days after the burst.

We will focus here on the extra absorption only, the evidence for which is fully confirmed - and strengthened - by *Swift* data. Indeed, adopting a simple, redshifted neutral absorption model, all datasets yield consistent values for both the redshift and the redshifted absorbing column, as well as of the spectral steepening as a function of time. *XMM-Newton* and *Swift*/XRT data point to a rather high redshift ($z \sim 4.2$) for GRB 090709A as well as to a huge column density in the host galaxy ($N_{\text{H}} \sim 6 \times 10^{22} \text{ cm}^{-2}$). Although a word of caution is required in considering such results (see Sect. 2.2.2), to our knowledge, this is the largest intrinsic absorption ever observed in an X-ray afterglow spectrum (see e.g. de Luca et al. 2005; Campana et al. 2006; Grupe et al. 2007).

This high absorption is also on the high side among expected column densities for sources located inside molecular clouds (Reichart & Price 2002). We note that part of the absorption could be due to intervening systems along the line of sight rather than being local to the host galaxy, as seen in the optical band in QSO and GRB studies (the so-called Damped Lyman- α Absorbers; Reichart & Price 2002; Wolfe et al. 2005). Lack of optical spectroscopy in the case of GRB 090709A prevents from drawing firm conclusions.

Such a picture suggests an explanation of the peculiar, very red colors of the infrared transient likely associated to GRB 090709A (Morgan et al. 2009) as due to reddening in the host galaxy. Indeed, if the GRB spectrum has no breaks in the X-ray to optical range and the redshift and intrinsic column derived from X-ray spectroscopy are correct, an extinction $A_V \sim 3$ in the GRB host galaxy (at $z = 4.2$) would fit the infrared data. This would point to a dust-to-gas ratio $\sim 10\%$ of that found in the Milky Way (assuming Solar abundances), similar to the findings of other investigations (e.g. Galama & Wijers 2001; Hjorth et al. 2003). Such an interpretation of the infrared data is possibly supported by the time decay of the infrared transient. The fading between the PAIRITEL and the Subaru observations is consistent with the $t^{-1.15}$ law describing the X-ray afterglow decay before the break at $T_0 + 0.26$ days, which suggests a common origin for the X-ray and infrared emission.

In any case, X-ray spectroscopy yields a robust indication that GRB 090709A was a very distant event.

4.2 On the prompt temporal variability

Coming back to the temporal properties of the prompt emission, our reanalysis, based on both *Swift*/BAT and *INTEGRAL* SPI/ACS data, could not confirm the presence of any significant signal at ~ 8.1 s. In any case, a complex multi-peaked light curve is clearly apparent, with a peak-to-peak separation of order ~ 8 – 10 s, and a peak at 0.125 Hz is present in the power spectrum derived from BAT data, just below the 3σ detection threshold. It is premature to comment on the apparent discrepancy between our results and those reported in a circular by Markwardt et al. (2009), in view of the lack of detailed information concerning the analysis performed by these authors. Indeed, several issues affect estimation of the significance of a signal when dealing with de-trending algorithms and Fourier transform techniques. Among the most important, we remember the presence of non-Poissonian noise in the power spectrum and the change in the statistical properties of a time series induced by operations such as subtraction and division. The former, if not taken into account properly, may result in an overestimation of the statistical significance of any peak sitting on a non-Poissonian underlying power spectrum continuum (see Israel & Stella 1996). The

latter affects the statistical properties of the original time-series. In particular, the division of a Poissonian variable (the time series) with a (model-dependent) de-trending algorithm might result in a non-Poissonian distributed time series with effects on the (unknown) statistical properties of the power spectrum noise.

The claimed period of about 8 s is precisely in the range of periods of soft gamma-ray repeaters (SGRs) and anomalous X-ray pulsars (AXPs). These sources are thought to be magnetars: isolated neutron stars powered by strong (10^{14} – 10^{15} G) magnetic fields (see Mereghetti 2008 for a review). Thus, association of GRB 090709A with the activity of a magnetar was suggested, also possibly based on some similarity of the light curve to the one of a magnetar giant flare, featuring a sort of “pulsating tail”.

Based on high energy properties, we can rule out such an interpretation. First, we could find no unambiguous, coherent pulsations in the γ -ray emission. Then, the spectrum of GRB 090709A is much harder than the typical spectra observed in the pulsating tails of the giant flares from SGRs. These are well described by thermal bremsstrahlung emission with $kT \sim 15$ – 30 keV, while the spectrum of GRB 090709A is typical for a GRB. Giant flares are also characterized by a short (< 0.5 s), very bright and spectrally hard initial spike that was clearly absent in GRB 090709A (although this feature was lacking in some “intermediate flares” from SGRs, all of them had a very sharp initial rise, contrary to the light curve of GRB 090709A). The location at high galactic latitude ($b \sim 20^\circ$) would also be very unusual for a Galactic SGR. Moreover, a Galactic origin may be safely ruled out by the observation of an absorbing column exceeding by a factor ~ 4 the Galactic value in the direction of GRB 090709A. A giant flare from an extragalactic SGR can also be excluded, based on the absence of a visible nearby galaxy at the location of GRB 090709A. The observed fluence would imply a distance not larger than 600 kpc (assuming an energetic similar to the one of other observed magnetar giant flares). The enormous energy requirement implied by a cosmological distance rules out the SGR giant flare hypothesis.

As already discussed in the previous section, we conclude that GRB 090709A is a standard, long GRB, with a multi-peak structure in the prompt emission. We will not go into pure speculations by considering physical processes that could produce a true quasi-periodic signal.

The variable prompt emission could be the signature of non-stationary processes in the GRB inner engine. As a likely possibility – discussed by Beskin et al. (2009) who observed a similar phenomenology in the optical emission from the “naked-eye” GRB 080319B (but with a possibly stronger evidence for quasi-periodicity) – the peculiar variability could be related to cyclic accretion by the central newborn compact object. Such a phenomenon could be due to the fragmentation of an accretion disc due to some kind of instability. For instance, Masada et al. (2007) explain short-time variability in the prompt emission by GRBs as due to magneto-rotational instabilities developing in a massive, hot hyperaccreting disc surrounding a central black hole of a few stellar masses. At a redshift $z \sim 4.2$, the variability time scale in the source frame would be of ~ 1.5 s. Thus, adopting the model of Masada et al. (2007), the observed properties of GRB 090709A could fit into such a scenario by assuming a beaming factor ~ 100 , for a $\sim 1 M_\odot$ accretion disc with inner radius of ~ 30 gravitational radii, surrounding a $\sim 4 M_\odot$ central black hole.

ACKNOWLEDGEMENTS

This research is based on observations obtained with *XMM-Newton* and *INTEGRAL*, which are both ESA science missions with instruments and contributions directly funded by ESA Member States and the USA (through NASA), and on observations with the NASA/UK/ASI *Swift* mission. We thank Norbert Schartel and the staff of the *XMM-Newton* Science Operation Center for performing the Target of Opportunity observation. The Italian authors acknowledge the partial support from ASI (ASI/INAF contracts I/088/06/0). DG acknowledges the CNES for financial support.

This paper has been typeset from a \TeX / \LaTeX file prepared by the author.

REFERENCES

- Aoki K., Ishii M., Kuzuhara M., Takahashi Y., Kawai N., 2009, GCN Circ., 9634
- Beskin G., Karpov S., Bondar S., Guarnieri A., Bartolini C., Greco G., Piccioni A., 2009, submitted to Science, preprint (arXiv: astro-ph/0905.4431)
- Buccheri R. et al., 1983, A&A, 128, 245
- Campana S. et al., 2006, A&A, 449, 61
- Castro-Tirado A. J. et al., 2009, GCN Circ., 9655
- Cenko S. B., Bloom J. S., Morgan A. N., Perley D. A., 2009, GCN Circ., 9646
- De Luca A. et al., 2005, A&A, 440, 85
- Dickey J. M., Lockman F. J., 1990, ARA&A, 28, 215
- Galama T. J., Wijers R. A. M. J., 2001, ApJ, 549, L209
- Golenetskii S., Aptekar R., Mazets E., Pal'Shin V., Frederiks D., Oleynik P., Ulanov M., Svinkin D., 2009, GCN Circ., 9647
- Götz D., Mereghetti S., von Kienlin A., Beck M., 2009, GCN Circ., 9649
- Grupe D., Nousek J. A., vanden Berk D. E., Roming P. W. A., Burrows D. N., Godet O., Osborne J., Gehrels N., 2007, AJ, 133, 2216
- Guidorzi C. et al., 2009, GCN Circ., 9648
- Hill J. E. et al., 2004, in Flanagan K. A., Siegmund O. H. W., eds, X-ray and Gamma-ray instrumentation for Astronomy XIII. Vol. 5165 of SPIE Conf. Ser., Bellingham WA, p 217
- Hjorth J. et al., 2003, ApJ, 597, 699
- Israel G. L., Stella L., 1996, ApJ, 468, 369
- Markwardt C. B., Gavril F. P., Palmer D. M., Baumgartner W. H., Barthelmy S. D., 2009, GCN Circ., 9645
- Masada Y., Kawanaka N., Sano T., Shibata K., 2007, ApJ, 663, 437
- Mereghetti S., 2008, A&A Rev., 15, 225
- Mirabal N., Gotthelf E. V., 2009, GCN Circ., 9696
- Morgan A. N., Bloom J. S., Klein C. R., 2009, GCN Circ., 9635
- Morris D. C. et al., 2009, GCN Circ., 9625
- Osborne J. P., Beardmore A. P., Evans P. A., Goad M. R., 2009, GCN Circ., 9636
- Reichert D. E., Price P. A., 2002, ApJ, 565, 174
- Rowlinson A., Morris D. C., 2009, GCN Circ., 9642
- Sakamoto T. et al., 2009, GCN Circ., 9640
- Senziani F., Novara G., de Luca A., Caraveo P. A., Belloni T., Bignami G. F., 2007, A&A, 476, 1297
- Stratta G., Fiore F., Antonelli L. A., Piro L., De Pasquale M., 2004, ApJ, 608, 846
- Vaughan B. A. et al., 1994, ApJ, 435, 362
- von Kienlin A. et al., 2003, A&A, 411, L299
- Wolfe A. M., Gawiser E., Prochaska J. X., 2005, ARA&A, 43, 861